INSTITUTE OF PLASMA PHYSICS

NAGOYA UNIVERSITY

RESEARCH REPORT

NAGOYA, JAPAN

COLLISIONLESS ELECTRON PLASMA WAVE SHOCKS*

K. Saéki, H. Ikezi and Y. Amagishi**

IPPJ- 163 May 1973

Further communication about this report is to be sent to the Research Information center, Institute of Plasma Physics, Nagoya University, Nagoya, JAPAN.

* Part of this paper is the thesis of K. Saéki.

** Permanent address: Department of Physics, Shizuoka University, Shizuoka, Japan.

Abstract

A large-amplitude electron plasma wave in a bounded collisionless plasma is observed to steepen and form a shock with a trailing wave train. The dependence of the Mach number and the period of the wave train on the shock amplitude shows that the shock structure is related to solitary waves. For a larger-amplitude shock, however, the trailing wave train is small or disappears, and a potential jump followed by large-amplitude oscillations propagating with a slower velocity than that of the shock front is observed. The amplitude of the oscillations is sufficiently large to trap a significant number of electrons and to form vortices in phase space.

§1. Introduction

Collisionless plasma shock waves have received considerable attention in recent years.[1] Since Taylor, Baker and Ikezi[2] established a method to generate large density perturbations in a plasma, the experimental,[3-7] numerical[8-11] and theoretical[12] studies of collisionless ion-acoustic shocks have been reported by many authors. The electron plasma wave shock reported here is essentially an electrostatic wave. However, it is different from the ion-acoustic shock in that only the electrons participate in its evolution.

Since the electron plasma wave in a cylindrical plasma[13] with a strong axial magnetic field has a dispersion relation, $(\omega/k_{\parallel})^2 = \omega_{pe}^2/(k_{\parallel}^2 + k_{\perp}^2)$, which is similar to that of the ion-acoustic wave, we would expect a shock wave similar to the ion-acoustic shock to be formed in the axial direction. Here, $k_{\parallel}$ and $k_{\perp}$ are the axial and perpendicular wave numbers, respectively. Indeed Manheimer[14] predicted theoretically that such a wave would steepen into a sharp density discontinuity. In that work, he neglected the coupling between the waves corresponding to different radial and azimuthal modes. An experiment[15] motivated by this anticipation has confirmed the existence of electron plasma wave shocks in the cylindrical plasma. This paper reports the details of a further experimental investigation.

§2. Experimental Conditions and Techniques

The experiments are performed in a single ended Q-

machine. The experimental setup is shown in Fig.1. The cylindrical conducting waveguide, 1.5 m long and 5.5 cm in diameter, is filled with a potassium plasma. Typical plasma parameters are as follows: plasma density $n \sim 10^7$ cm^{-3}; electron temperature $T_e \simeq 0.4$ eV; background neutral gas pressure $p \sim 1 \times 10^{-6}$ Torr, and static axial magnetic field B = 3 kG. For these values of the parameters, electron mean-free-path is much longer than the length of the waveguide. Since the electron cyclotron frequency ω_{ce} is much higher than the electron plasma frequency ω_{pe}, the phase velocity u_o given by $\omega_{pe}/k_\perp$ for $\omega << \omega_{pe}$, is (2 - 3) $\times 10^8$ cm/sec. Here $k_\perp = 2.4/a$, where a is the radius of the waveguide. The electron thermal velocity is about 3×10^7 cm/sec.

The wave exciter is at the opposite end of the plasma from the hot plate which generates the plasma. Conventional probe or grid[16] excitation is not used for the following reason. In order to create large amplitude electron density perturbations in the plasma, the wave exciter must be able to supply a significant amount of excess electrons into the plasma. This is the idea suggested by the method employed in the experiment[2] on ion-acoustic wave shocks. In that case, the wave exciter was actually an ion source. Two types of wave exciters ("Type A" and "Type B") are used in the present experiments. Type A, shown in Fig.1, consists of a barium-oxide coated cathode, 5 cm in diameter, and a mesh grid separated from the cathode by 5 mm. The grid is directly connected to the waveguide and has the function

of extracting electrons from the cathode. The excitation of a ramp wave, which is used for observing the wave steepening, is accomplished as follows. First, the electron injection is inhibited by biasing the cathode at the plasma potential. Then at t = 0, a negative ramp potential is applied to the cathode and the electrons, which give rise to the electron density perturbation are injected into the plasma. Both the amplitude of the ramp potential ϕ_{ex} and its rise time t_r can be varied. The Type B exciter is simply a conducting cylinder which has the same diameter as that of the waveguide and is 50 cm in length. The cylinder is filled by the plasma as well as the waveguide where we observe the shocks. Applying a negative potential ϕ_{ex} to the cylinder causes the plasma electrons contained in it to be injected into the plasma.

The wave potential is detected with a wire probe which is connected to a high input resistance circuit[16] which responds in a frequency range from 0.1 MHz to 100 MHz. Since this is a capacitive input impedance circuit, we can measure the absolute amplitude of the wave potential ϕ. We estimate the thickness of the sheath around the probe to be $4\lambda_D$.[17]

§3. Experimental Results

3.1 Small-Amplitude Wave

Before describing the shock wave results, we first examine the features of the small-amplitude wave. Figure 2 shows the spatial wave response at a fixed time due to a

1 V step excitation. The rise time of the step is much shorter than $2\pi/\omega_{pe}$. The plots are obtained by sampling the wave potential signal from the probe at a fixed time t, while sweeping the probe position axially. The repetition frequency of the step voltage is typically 100 kHz. A wave train results behind the wave front. The wavelength, $(10 \sim 20)k_{\perp}^{-1}$, of the wave train expands as it propagates, proportional to $t^{1/3}$.

The velocity of the wave front, 1.9×10^8 cm/sec, is much faster than the electron thermal velocity, 2.6×10^7 cm/sec, therefore Landau damping is not observable. Interferometer measurements of the small amplitude monochromatic waves show that the above velocity of the front agrees with the phase velocity of the wave when $\omega << \omega_{pe}$. The wave amplitude $e\phi/mu_o^2$ ($u_o = \omega_{pe}/k_{\perp}$) is about 0.04. If the plasma density is reduced, the wave velocity decreases and the wave trains disappear as the velocity approaches the electron thermal velocity; i.e., they suffer Landau damping. No higher radial nor azimuthal modes are observable under the present experimental conditions. Using either type of wave exciter does not make a significant difference in the features of the small-amplitude waves.

3.2 Steepening

Figure 3(a) shows the nature of the compressional-wave propagation due to the applied potential ramp shown in the bottom trace. The excess electrons are injected by the Type A exciter. The negative potential corresponds to a

compressional wave because of the negative sign of the electron charge. As the wave propagates, it steepens and is followed by a wave train with a frequency $\sim 0.5\ \omega_{pe}$. A small precursor can be seen in front of the shock. The amplitude of the precursor is found to become smaller when the wave amplitude becomes smaller, or when the plasma density increases such that the shock velocity becomes faster. The experiment in the lower density plasma shows that no wave train results. Large-amplitude sinusoidal waves are also observed to steepen as shown in Fig.3(b).

The possibility of spurious effects due to the streaming electrons from the cathode is checked in the following way. When the plasma is turned off and only electrons are injected from the cathode into the vacuum by the step potential (top trace in Fig.4) applied to the cathode, the leading edge of the streaming electrons is observed to spread as it travels (see second trace). If the plasma is turned on, then the shock wave forms. As the plasma density is increased, the shock-wave velocity increases (see bottom trace). Since the velocity of the streaming electrons leaving the wave exciter is fixed, this dependence of the shock velocity on the plasma density excludes the possibility of steepening due to bunching of the streaming electrons. These observations also show that the precursor consists partially of the electrons from the wave exciter freely streaming into the plasma.

All experimental observations show that the compressional waves steepen in a time

$$t_s = t_r \frac{m u_o^2}{e \phi_{max}} \qquad (1)$$

within an error of 30% provided the ramp rise time $t_r > \omega_{pe}^{-1}$. Here, ϕ_{max} is the maximum potential amplitude of the wave. The derivation of Eq.(1) will be given in the next section.

The type B exciter generates both the compressional and the rarefaction waves. If a negative ramp is applied to the cylinder, the compressional wave is launched into the waveguide and propagates away from the boundary between the waveguide and the cylinder, and the rarefaction wave propagates in the cylinder. Since the cylinder is essentially a waveguide, the application of the positive ramp generates a wave of opposite polarity. It is observed that the compressional waves excited by the Type B exciter steepen into shock waves and show essentially the same behavior as those launched by Type A. The rarefaction waves are found to spread rather than steepen.

3.3 Structure of the Shocks

The structure of the shock depends primarily on its amplitude. For small amplitudes, a slow wave train appears as already noted in Fig.2. Fig.5(a) shows the spatial wave response at a fixed time (= 0.5 μs) due to a step excitation with the Type A exciter. As the excitation amplitude is increased, the shock front shifts to the right (i.e., the Mach number increases) and the period of the wave train shortens. In contrast to the case of very small amplitude

waves, the period of the wave trains behind the larger amplitude shock does not change very much during their propagation. The wave number of the wave train k and the Mach number $M(\equiv u/u_o)$ are plotted in Fig.6 as a function of the maximum amplitude of the shock, ϕ_{max}. Here, u is the shock velocity. The values of k plotted in this figure are obtained from the separation between the first two peaks when t = 0.35 μs. Since the period of the wave train increases as it propagates when the amplitude is small, the values of k are smaller than those plotted in Fig.6 if we use the data obtained at larger t.

The properties described above are observed when ϕ_{ex} is not very large. Let us return to Fig.5(a). Increasing ϕ_{ex} eliminates the wave train and increases the amplitude of the precursor, and finally the wave jumps up behind the shock front when ϕ_{ex} exceeds $mu_o^2/2e$ [= 14 V in the case of Fig.5(a)]. The observation of the propagation direction shows that this jump is not due to any interference with the wave reflected from the control grid. Behind the potential jump, noise grows, presumably due to an electron two-stream instability. In the small-amplitude range where the shock with its wave train is formed, the amplitude of the shock ϕ_{max} is proportional to the excitation potential ϕ_{ex}. After ϕ_{ex} reaches the value at which the wave train disappears, ϕ_{max} saturates.

When ϕ_{ex} applied to the Type B exciter is not very large, there is no difference in the shock structure from that produced by the Type A exciter. The potential jump

is also created when ϕ_{ex} exceeds $mu_o^2/2e$ [= 8.3 V in the case of Fig.5(b)]. However, in contrast with the shock excited by the Type A exciter, the potential jump is followed by a large amplitude and long wavelength oscillations, and no random noise grows. It should also be noted that the wave train behind the shock does not vanish. No shock wave is observed when ϕ_{ex} exceeds 33 V [$\simeq 2mu_o^2/e$] in Fig.5(b). The upper critical Mach number is observed to be 1.25.

The oscillations behind the potential jump may be more easily observed temporarily. Fig.7 shows their growth, parameterized by the axial distance from the exciter. At small distances, only a single potential hump is seen. As the shock propagates, the interval between the shock front and the potential jump lenghthens and the number of oscillations increases. The amplitude of the oscillation is about the same as that of the shock front. We observe that two oscillations would occasionally coalesce into a single, longer-period oscillation.

3.4 Comparison to the Grid Excitation

In closing this section, we compare the difference between the conventional grid or probe excitation method and the method used in these experiments. As reported in Ref.16, the grid or the probe does not generate a shock wave which has a DC potential jump, even for a step excitation. The same result is confirmed in the present experiment. This is due to the fact that the probe or the grid

can not supply electrons continuously into the plasma because it is not an electron source. On the other hand, the exciters which we have used here can be electron sources and can therefore launch waves which have the same waveform of the wave potential as that of the applied potential signal.

§4. Analysis and Discussions

It has been shown that the evolution of small but finite amplitude Trivelpiece-Gould waves[13,14] is described by the Kortweg-deVries equation† (see Appendix).

$$\frac{\partial \psi}{\partial \tau} - \frac{3}{2}\alpha\psi\frac{\partial \psi}{\partial \xi} + \frac{1}{2}\frac{\partial^3 \psi}{\partial \xi^3} = 0, \qquad (2)$$

if we neglect the coupling to the higher-order perpendicular modes and the thermal motion of the electrons. Here,

$$\psi = \frac{e\phi}{mu_0^2}, \quad \tau = \omega_{pe}t,$$
$$\xi = k_\perp z - \omega_{pe}t$$

and

$$\alpha = \int_0^{2.4} J_0^3(r)\,r\,dr \Big/ \int_0^{2.4} J_0^2(r)\,r\,dr = 0.72,$$

† In the derivation of the Kortweg-deVries equation in Ref.16, the radial mode is not treated properly. However, the final expression is correct as long as the coupling between the different radial modes is neglected.

4.1 Small-Amplitude Wave

We first analyze the structure of the small-amplitude wave. We solve Eq.(2), neglecting the nonlinear term and setting the initial condition to be

$$\psi(0,\xi) = \begin{cases} \psi_0 , & \xi \le 0 \\ 0 , & \xi > 0 \end{cases} \qquad (3)$$

at $\tau = 0$. We Fourier transform Eq.(2) in ξ and Laplace transform it in τ. After some simple calculations, the inverse transforms give us

$$\psi(\tau,\xi) = \frac{\psi_0}{\pi} \int_{\xi/(\tau/2)^{1/3}}^{\infty} A_i(x)\,dx , \qquad (4)$$

where Ai is the Airy function. Equation (4) agrees with the solution of the linearized piston problem for ion-acoustic waves.[18] The plot of ψ as a function of z with t as a parameter agrees well with the waveform shown in Fig.2. Since ψ is a function of $\xi/(\frac{\tau}{2})^{1/3} = (k_\perp z - \omega_{pe} t)/(\frac{1}{2}\omega_{pe} t)^{1/3}$ the period of the wave train increases proportionally with $t^{1/3}$. Equation (2) contains only the lowest-order dispersion effects. Its solution does not completely describe the waveform far behind the wave front where the large wavenumber components determine the wave's shape. However, such large wavenumber components are quickly Landau damped. Therefore the solution of the fluid equation does not apply.

4.2 Steepening Time

The second term of Eq.(2) accounts for wave steepening.

A gentle initial potential profile such that the third term of Eq.(2) may be neglected will be considered. We analyze the steepening by employing the characteristics defined by

$$\frac{d\xi}{d\tau} = -\frac{3\alpha}{2}\psi . \qquad (5)$$

It is assumed that a negative potential ramp at t = 0 is applied to the wave exciter at z = 0. The ramp rises until a time t_r and excites a wave with a maximum amplitude $-\phi_{max}$. Two characteristics can be drawn in the τ - ξ plane. One of them starts from $\tau = \xi = 0$ with a slope $d\xi/d\tau = 0$, and the other starts from $\tau = -\xi = \omega_{pe} t_r$ with a slope $d\xi/d\tau = (3\alpha/2)\psi_{max}$ where $\psi_{max} = e\,\phi_{max}/mu_o^2$. As shown by the line (a) in Fig.8, one characteristic crosses the other and leads to a potential discontinuity. The steepening time is calculated as

$$t_s = \left(\frac{2}{3\alpha}\frac{mu_o^2}{e\phi_{max}} + 1\right) t_r \simeq \frac{mu_o^2}{e\phi_{max}} t_r . \qquad (6)$$

If a positive ramp is applied, then the two characteristics separate from each other and lead to a spreading of the wave (line (b)). The dependence of t_s on ϕ_{max} indicated in Eq.(6) is confirmed quantitatively in the experiments. However, once the wave steepens, the wave dispersion effect limits the steepening and the sharp potential discontinuity does not appear. This fact introduces the main source of experimental error when we measure t_s.

4.3 Mach Number and Wave Train

We compare the observed dependence of the Mach number M ($\equiv u/u_o$) and the wave number of the wave train k on the shock amplitude with the prediction of the stationary-state solution of Eq.(2). Although Eq.(2) does not have a shock wave solution, dissipation or electron reflection will result in shock formation.[19-21] We define a new variable

$$\eta = \xi - \Delta M \tau , \qquad (7)$$

and assume ψ is a function of η. After integration by η, Eq.(2) is reduced to

$$\frac{1}{2}\left(\frac{d\psi}{d\eta}\right)^2 + U(\psi) = 0 , \qquad (8)$$

where

$$U = -\Delta M \psi^2 - \frac{\alpha}{2}\psi^3 .$$

We have assumed $d^2\psi/d\eta^2 = 0$ when $\psi = 0$. The function U has a minimum at $\psi_o = -4\Delta M/3\alpha$ and ψ changes following the pseudo-potential U. At $\eta = \infty$, ψ starts from $\psi = 0$ and goes negative. If there is no dissipation, then Eq.(8) leads to a solitary wave. However, the breaking of charge neutrality due to electron reflection introduces oscillations of ψ around ψ_o. We calculate the oscillation period which corresponds to k. Expanding U about its minimum, we obtain a harmonic-oscillator equation, from which k is estimated to be

$$\frac{k}{k_\perp} = \left(\frac{\alpha e \phi_{max}}{m u_o^2} \right)^{\frac{1}{2}}, \qquad (9)$$

Eq.(8) also gives the relation

$$\Delta M \equiv M - 1 = \frac{\alpha}{2} \frac{e\phi_{max}}{m u_o^2} , \qquad (10)$$

A calculation employing a better approximation[16] leads to a slightly improved relation

$$M^2 (M^2 - 1) = \alpha \frac{e\phi_{max}}{m u_o^2} . \qquad (11)$$

The solid curves in Fig.6 calculated from (9) and (11) both fit the experimental points reasonably well. When $e\phi_{max}$ exceeds 0.4 mu_o^2, the wave train disappears and significant number of reflected and transmitted electrons are observed. Therefore, the above analysis which neglects wave-particle interactions would not be applicable in this high-amplitude limit.

4.4 Strong Shocks

When the amplitude of the potential ϕ_{ex} applied to the wave exciter is greater than $mu_o^2/2e$, the following behavior of the shock is observed: (i) A large potential jump appears behind the shock. This potential jump is not a higher-order perpendicular mode since its velocity is slower in the higher density plasma. (ii) The amplitude of the potential jump increases with ϕ_{ex}. (iii) Large-amplitude

oscillations of frequency $\omega_{pe}/(2 - 3)$ follow the potential jump. The amplitude of the oscillations is about the same as that of the shock. (iv) No shock wave is observed when ϕ_{ex} exceeds $\sim 2mu_o^2/e$.

No analytical interpretation has been attempted so far. We find, however, great similarities between the waveforms observed in the present experiment (Fig.7) and those obtained in the numerical simulation by Sakanaka.[11] He has treated the ion-acoustic shocks, in which the dynamics of the ions dominate the evolution of the wave and the electrons shield the ion space charge. In the present electron wave, the space charge resulting from the electron perturbation is shielded by the surface charge induced on the surrounding metallic waveguide. Therefore we may employ the results obtained for the ion-acoustic waves if we make the following transformations: $\omega_{pi} \rightarrow \omega_{pe}$, $k_D \rightarrow k_\perp$, and ion-acoustic velocity $\rightarrow u_o$. The difference between the two cases is that the computation is carried out in one-dimension whereas the waves in the waveguide is three-dimensional.

The initial condition in Sakanaka's numerical analysis is as follows: The ions have a two-component distirbution; one component is uniform background ions; the other is a uniform "beam" which occupies only the left half-space with a positive flow velocity. He has observed that a region where the ions are accumulated grows and expands in space and large-amplitude oscillations develop behind it. The pictures of the ion distribution in phase space show that the oscillations consist of vortices. Numerical work by

Kamimura[22] has shown that two vortices coalesce to form one vortex.

The large-amplitude excitation potential in our experiments injects an electron-beam into the plasma. If we follow the evolution of the electron distribution instead of the ions, the behavior of the wave shown in Fig.7 is thought to be essentially the same as that described in the above numerical works. Indeed, the observed potential amplitude of the oscillations is sufficiently large for the trapping of the electron-beam.

§5. Conclusions

An electron plasma wave in a bounded collisionless plasma is observed to steepen and to form a shock wave with a trailing wave train. When the amplitude of the shock is small, the solution of the linearized piston problem qualitatively accounts for the wave form. As the wave amplitude increases, the Mach number increases and the wavelength of the wave train decreases. An analysis based on the Kortweg-deVries equation describes the dependence of the wavenumber of the train and the Mach number on the shock amplitude. When a very large excitation potential is applied to the wave exciter, the amplitude of the precursor increases and a potential jump followed by large-amplitude oscillations grows. The amplitude of the oscillations is sufficiently large to trap electrons injected from the wave exciter. Comparison with a numerical work suggests that the oscillations form vortices in phase space.

Acknowledgements

The authors are very grateful to Professor J. M. Dawson for his suggesting the idea of the Type B exciter. They also appreciates helpful discussions with Professor T. Taniuti and Professor B. D. Fried.

APPENDIX

In this appendix we will derive the Kortweg-deVries equation for the electron plasma wave propagating in a cylindrical waveguide. We assume the plasma is uniform in the waveguide. We consider the case when very strong axial magnetic field is applied to the plasma, so that the electrons can move only axial direction (z-direction). We also assume $T_e = 0$ and start from the fluid equations:

$$\left.\begin{aligned} &\frac{\partial v}{\partial t} + v\frac{\partial v}{\partial z} - \frac{e}{m}\frac{\partial \phi}{\partial z} = 0 , \\ &\frac{\partial n}{\partial t} + \frac{\partial}{\partial z}(nv) = 0 , \\ &\nabla_\perp^2 \phi + \frac{\partial^2 \phi}{\partial z^2} = 4\pi e(n - n_0) . \end{aligned}\right\} \qquad (A1)$$

Here v is the axial electron fluid velocity, n the electron density, ϕ the potential. Ions are treated as an uniform background and their density is n_o.

First, we linearize (A1) and obtain an equation for the potential

$$\left(\nabla_\perp^2 + \frac{\partial^2}{\partial z^2}\right)\frac{\partial^2 \phi}{\partial t^2} = -\omega_{pe}^2 \frac{\partial^2 \phi}{\partial z^2} . \qquad (A2)$$

Separating variables

$$\phi = f(r,\theta)\exp[i(kz - \omega t)] , \qquad (A3)$$

(A2) is written as

$$\left[(\nabla_\perp^2 - k^2)\omega^2 + \omega_{pe}^2 k^2 \right] f(r,\theta) = 0 . \qquad (A4)$$

The solution of (A4) may be expanded by the eigen functions as

$$f(r,\theta) = \sum_{m,n} \Psi_{m,n} J_n(k_{mn} r) e^{in\theta}$$

$$\equiv \sum_{m,n} \Psi_{mn} R_{mn}(r,\theta) . \qquad (A5)$$

The waveguide sets $\phi = 0$ at $r = a$, so that

$$J_n(k_{mn} a) = 0 . \qquad (A6)$$

Once radial wavenumber k_{mn} is determined by (A6), the linear dispersion relation is known from (A4).

Now let us derive approximate nonlinear equation for ϕ. For simplicity we rewrite variables as follows:

$$\frac{n}{n_0} \to n , \quad \frac{e\phi}{m\left(\frac{\omega_{pe}}{k_{00}}\right)^2} \to \phi , \quad \frac{V}{(\omega_{pe}/k_{00})} \to V$$

$$k_{00} z \to z , \quad \text{and} \quad \omega_{pe} t \to t . \qquad (A7)$$

Then a set of equations (A1) is written as

$$\frac{\partial V}{\partial t} + V \frac{\partial V}{\partial z} - \frac{\partial \phi}{\partial z} = 0 , \qquad]$$

$$\left.\begin{aligned} &\frac{\partial n}{\partial t} + n\frac{\partial V}{\partial z} + V\frac{\partial n}{\partial z} = 0 \quad , \\ &\left(\frac{1}{k_{oo}^2}\nabla_\perp^2 + \frac{\partial^2}{\partial z^2}\right)\phi = n - 1 . \end{aligned}\right\} \qquad (A8)$$

The normarizations (A7) indicate that we are interested in the fundamental perpendicular mode which corresponds to k_{oo}. Following the method employed by Washimi and Taniuti,[18] we introduce new coordinate system (ξ, τ) which is defined by the transformation:

$$\tau = \epsilon^{\frac{3}{2}} t \quad , \quad \text{and} \quad \xi = \epsilon^{\frac{1}{2}}(z - ut) \qquad (A9)$$

wehre ϵ is a small parameter of the order of magnitude of the wave amplitude. In the new coordinate system, (A8) is

$$\left.\begin{aligned} &\epsilon\frac{\partial V}{\partial \tau} - u\frac{\partial V}{\partial \xi} + V\frac{\partial V}{\partial \xi} - \frac{\partial \phi}{\partial \xi} = 0 , \\ &\epsilon\frac{\partial n}{\partial \tau} - u\frac{\partial n}{\partial \xi} + n\frac{\partial V}{\partial \xi} + V\frac{\partial n}{\partial \xi} = 0 , \\ &\left(k_{oo}^{-2}\nabla_\perp^2 + \epsilon\frac{\partial^2}{\partial \xi^2}\right)\phi = n - 1 . \end{aligned}\right\} \qquad (A10)$$

We expand v, n and ϕ as

$$\left.\begin{aligned} n &= 1 + \epsilon\sum_{m,n} R_{mn}\, n_{mn}^{(1)} + \epsilon^2 \sum_{m,n} R_{mn}\, n_{mn}^{(2)} + \cdots \\ V &= \epsilon\sum_{m,n} R_{mn}\, V_{mn}^{(1)} + \epsilon^2 \sum_{m,n} R_{mn}\, V_{mn}^{(2)} + \cdots \\ \phi &= \epsilon\sum_{m,n} R_{mn}\, \phi_{mn}^{(1)} + \epsilon^2 \sum_{m,n} R_{mn}\, \phi_{mn}^{(2)} + \cdots \end{aligned}\right\} \qquad (A11)$$

Substituting (A11) into (A10) and collecting terms of order ε, we have

$$\sum_{m,n} \frac{R_{mn}}{u_{mn}} \frac{\partial V_{mn}^{(1)}}{\partial \xi} = \sum_{m,n} R_{mn} \frac{\partial n_{mn}^{(1)}}{\partial \xi} = -\sum_{mn} \frac{R_{mn}}{u_{mn}^2} \frac{\partial \phi_{mn}^{(1)}}{\partial \xi}, \quad (A12)$$

where

$$u_{mn} = \frac{k_{cc}}{k_{mn}} . \quad (A13)$$

Using the condition $n_{mn}^{(1)} = v_{mn}^{(1)} = 0$ where $\phi_{mn}^{(1)} = 0$, we integrate (A12) and obtain

$$u_{mn}^{-1} V_{mn}^{(1)} = n_{mn}^{(1)} = - u_{mn}^{-2} \phi_{mn}^{(1)} . \quad (A14)$$

The equations of the order ε^2 are

$$\left.\begin{aligned}
&\sum_{m,n} R_{mn} \left(\frac{\partial V_{mn}^{(1)}}{\partial \tau} - u_{mn} \frac{\partial V_{mn}^{(2)}}{\partial \xi} + \sum_{m',n'} R_{m'n'} \frac{\partial V_{m'n'}^{(1)}}{\partial \xi} V_{mn}^{(1)} \right. \\
&\qquad \left. - \frac{\partial \phi_{mn}^{(2)}}{\partial \xi} \right) = 0 , \\
&\sum_{m,n} R_{mn} \left[\frac{\partial n_{mn}^{(1)}}{\partial \tau} - u_{mn} \frac{\partial n_{mn}^{(2)}}{\partial \xi} + \frac{\partial V_{mn}^{(2)}}{\partial \xi} \right. \\
&\qquad \left. + \sum_{m',n'} R_{m'n'} \left(\frac{\partial V_{m'n'}^{(1)}}{\partial \xi} n_{mn}^{(1)} + \frac{\partial n_{m'n'}^{(1)}}{\partial \xi} V_{mn}^{(1)} \right) \right] = 0 , \\
&\sum_{m,n} R_{mn} \left(- \frac{k_{mn}^2}{k_\infty^2} \phi_{mn}^{(2)} + \frac{\partial^2 \phi_{mn}}{\partial \xi^2} \right) = \sum_{m,n} R_{mn} n_{mn}^{(2)} .
\end{aligned}\right\} \quad (A15)$$

Now we concentrate to the behavior of the fundamental radial mode, namely m = n = 0. In order to obtain the equation for ϕ_{oo}, we multiply R_{oo} to all equations and integrate over the cross-section of the wave guide,

i.e., $\int_0^a r dr \int_0^{2\pi} d\theta$,

$$\left.\begin{aligned}
&\frac{\partial V_{oo}^{(1)}}{\partial \tau} - \frac{\partial V_{oo}^{(2)}}{\partial \xi} + \sum_{p,q} \gamma_{pq} V_p^{(1)} \frac{\partial V_q^{(1)}}{\partial \xi} - \frac{\partial \phi_{oo}^{(2)}}{\partial \xi} = 0, \\
&\frac{\partial n_{oo}^{(1)}}{\partial \tau} - \frac{\partial n_{oo}^{(2)}}{\partial \xi} + \frac{\partial V_{oo}^{(2)}}{\partial \xi} + \sum_{p,q} \gamma_{pq} n_p^{(1)} \frac{\partial V_q^{(1)}}{\partial \xi} \\
&\qquad + \sum_{p,q} \gamma_{pq} V_p^{(1)} \frac{\partial n_q^{(1)}}{\partial \xi} = 0, \\
&\frac{\partial^2 \phi_{oo}^{(1)}}{\partial \xi^2} = \phi_{oo}^{(2)} + n_{oo}^{(2)}.
\end{aligned}\right\} \quad (A16)$$

where p = (m, n), q = (m', n') and

$$\gamma_{pq} = \frac{\int_0^a r dr \int_0^{2\pi} d\theta \, R_{oo} R_{mn} R_{m'n'}}{2\pi \int_0^a r dr \, R_{oo}^2}, \quad (A17)$$

As Manheimer discussed,[14] the value of $\gamma_{(o,o)(o,o)}$ is much larger than any other γ. Therefore we neglect coupling to the higher-order perpendicular modes. With the aid of (A14), we obtain

$$\frac{\partial \phi_{oo}^{(1)}}{\partial \tau} - \frac{3\alpha}{2} \phi_{oo}^{(1)} \frac{\partial \phi_{oo}^{(1)}}{\partial \xi} + \frac{1}{2} \frac{\partial^3 \phi_{oo}^{(1)}}{\partial \xi^3} = 0, \quad (A18)$$

where $\alpha = \gamma_{(o,o)(o,o)}$.

REFERENCES

1. D. A. Tidman and N. A. Krall, *Shock Waves in Collisionless Plasmas* (Wiley, New York, 1971).
2. R. J. Taylor, D. R. Baker and H. Ikezi, Phys. Rev. Lett. 24 (1970) 206.
3. H. Ikezi, R. J. Taylor and D. R. Baker, Phys. Rev. Lett. 25 (1970) 11.
4. A. Y. Wong and R. W. Means, Phys. Rev. Lett. 27 (1971) 973.
5. R. A. Stern and J. F. Decker, Phys. Rev. Lett. 27 (1971) 1266.
6. S. G. Alikhanov et al., Sov. Phys. JETP 33 (1971) 532.
7. D. Cohn and K. R. MacKenzie, Phys. Rev. Lett. 28 (1972) 656.
8. D. W. Forslund and C. R. Shonk, Phys. Rev. Lett. 25 (1970) 1699.
9. D. W. Forslund and J. P. Freidberg, Phys. Rev. Lett. 27 (1971) 1189.
10. P. H. Sakanaka, C. K. Chu and T. C. Marshall, Phys. Fluids 14 (1971) 611.
11. P. H. Sakanaka, Phys. Fluids 15 (1972) 304, 1323.
12. R. B. White, B. D. Fried and F. V. Coroniti, Phys. Fluids 15 (1972) 1484.
13. A. W. Trivelpiece and R. W. Gould, J. Appl. Phys. 30 (1959) 1784.
14. W. M. Manheimer, Phys. Fluids 12 (1969) 2426.

FIGURE CAPTIONS

Fig.1. Experimental setup. Wave exciters are shown schematically at the bottom.

Fig.2. Spatial plot of wave potential with time after the small voltage step ϕ_{ex} as a parameter. Type A exciter is used. ϕ_{ex} = -1 V, and n = 9.0×10^5 cm^{-3}.

Fig.3. Plot of wave potential versus time with distance as a parameter, excited by ramp signal (a) and by sinusoidal signal (b). The wave potential signals in this figure and also Fig.s 4 and 7 are delayed by 0.05 μs in the cables from the pulse oscillator to the wave exciter and from the receiver probe to the scope.

Fig.4. Effect of streaming electrons from the Type A exciter on the shock at different plasma densities, observed at z = 100 cm.

Fig.5. Spatial plot of the wave potential with amplitude of the excitation step as a parameter. (a) Type A exciter is employed. n = 1.2×10^7 cm^{-3}, $mu_o^2/2e$ = 14 V. The time t is fixed at 0.5 μs after the step. (b) Type B exciter is employed. n = 7.2×10^6 cm^{-3}, $mu_o^2/2e$ = 8.3 V, and t = 0.6 μs.

Fig.6. Dependence of wave number of the wave train at t = 0.35 μs, and Mach number on shock amplitude. n = 1.7×10^7 cm^{-3}.

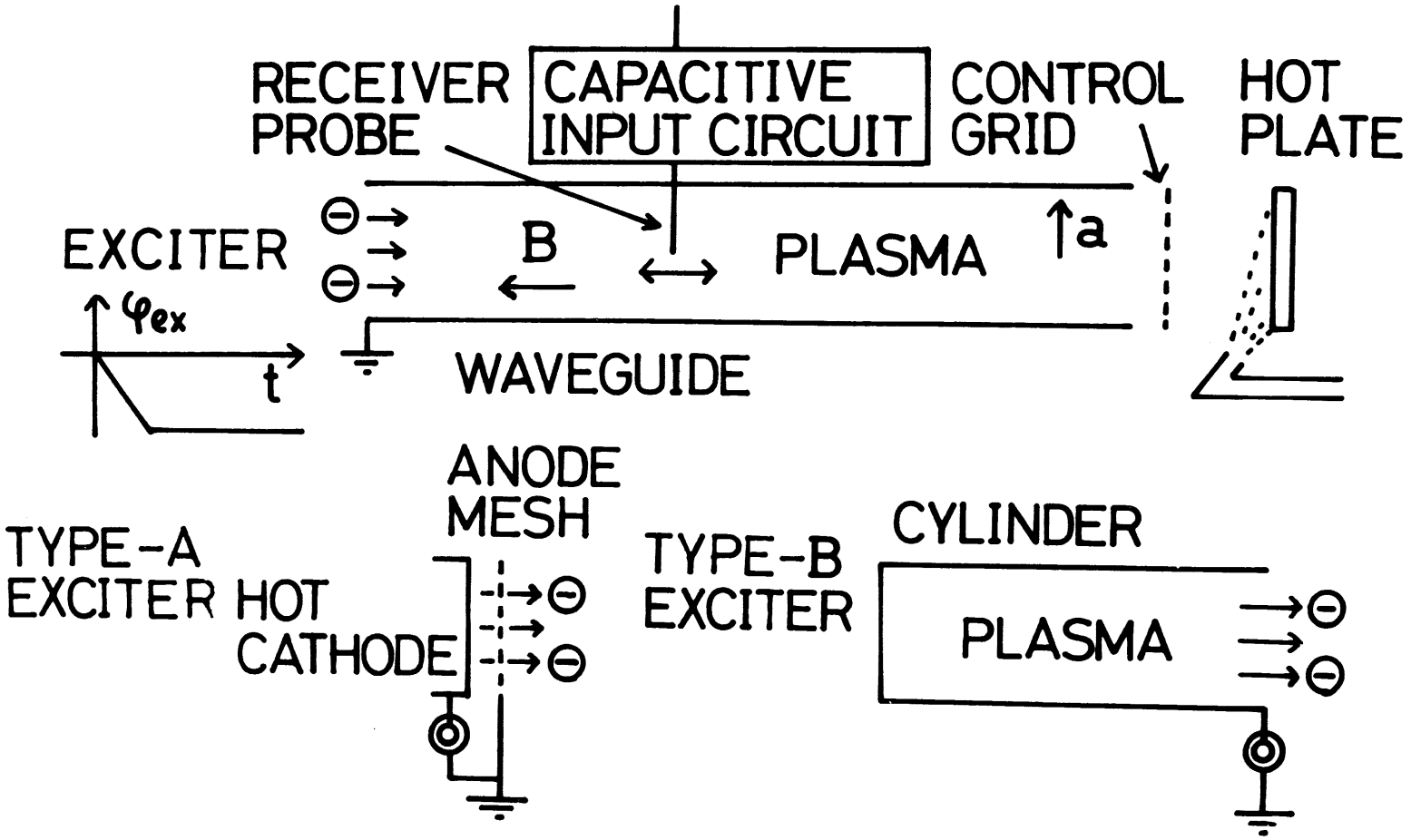
RECEIVER PROBE
CAPACITIVE INPUT CIRCUIT
CONTROL GRID
HOT PLATE
EXCITER
B
PLASMA
a
φex
t
WAVEGUIDE
ANODE MESH
TYPE-A EXCITER
HOT CATHODE
TYPE-B EXCITER
CYLINDER
PLASMA

Fig. 1

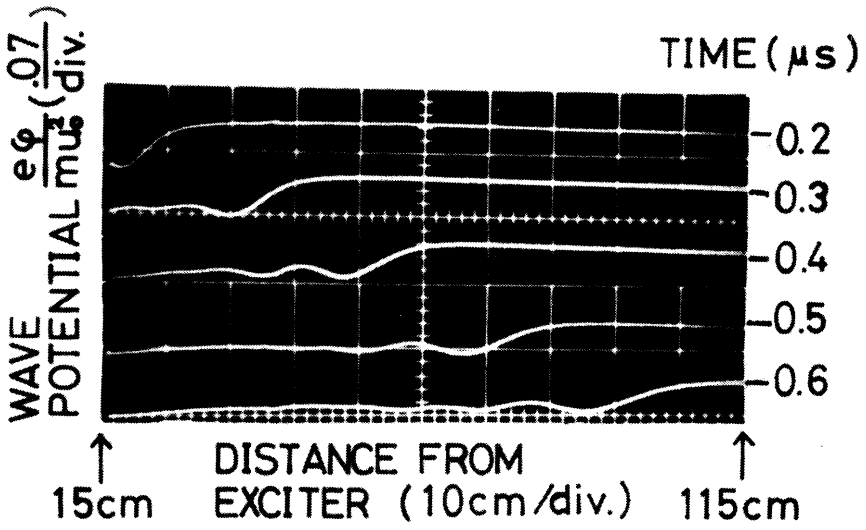
WAVE POTENTIAL eφ/mu₀³ (.07/div.)
TIME (μs)
0.2
0.3
0.4
0.5
0.6
15cm
DISTANCE FROM EXCITER (10cm/div.)
115cm

Fig. 2

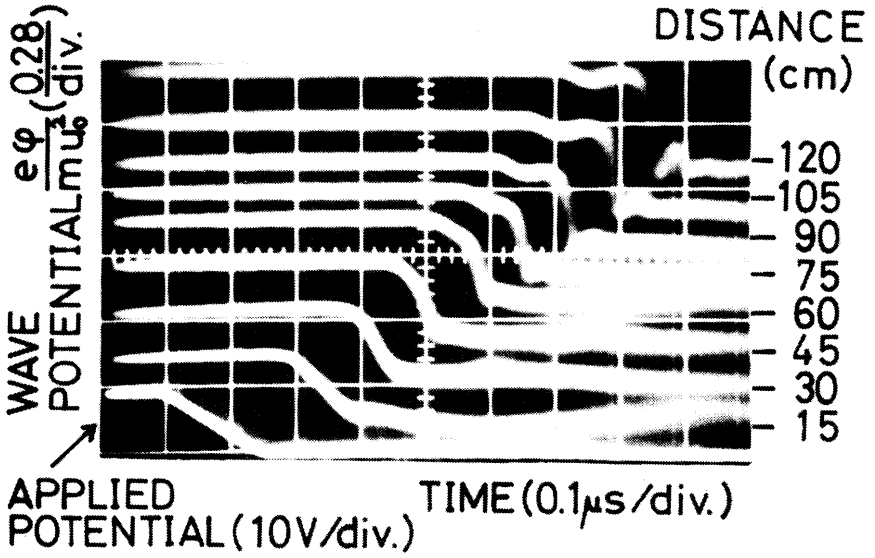
DISTANCE
(cm)
120
105
90
75
60
45
30
15
WAVE POTENTIAL $\frac{e\varphi}{mu_0^2}$ (0.28/div.)
APPLIED POTENTIAL (10V/div.)
TIME (0.1μs/div.)

(a)

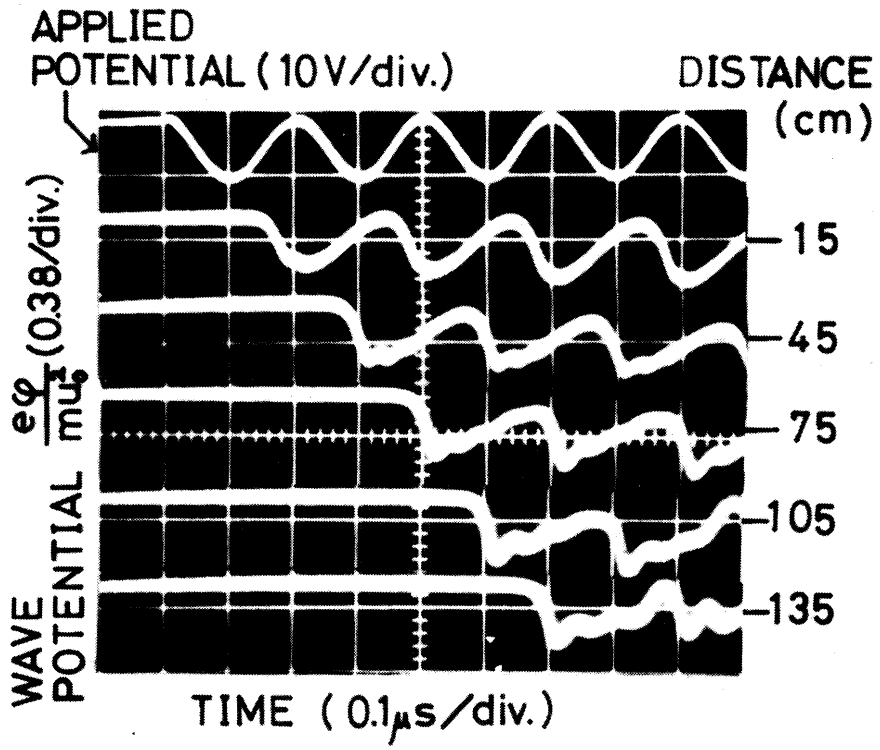
APPLIED POTENTIAL (10V/div.)
DISTANCE
(cm)
15
45
75
105
135
WAVE POTENTIAL $\frac{e\varphi}{mu_0^2}$ (0.38/div.)
TIME (0.1μs/div.)

(b)

Fig. 3

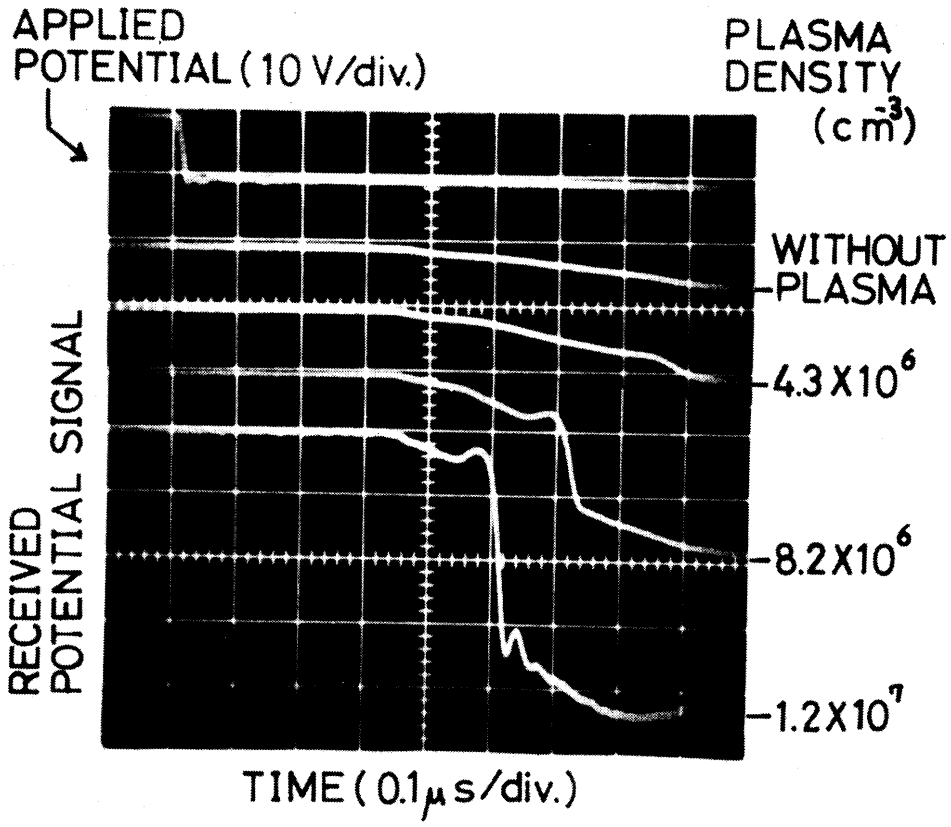
APPLIED
POTENTIAL (10 V/div.)
PLASMA
DENSITY
(cm⁻³)
WITHOUT
PLASMA
4.3X10⁶
8.2X10⁶
1.2X10⁷
RECEIVED
POTENTIAL SIGNAL
TIME (0.1μs/div.)

Fig. 4

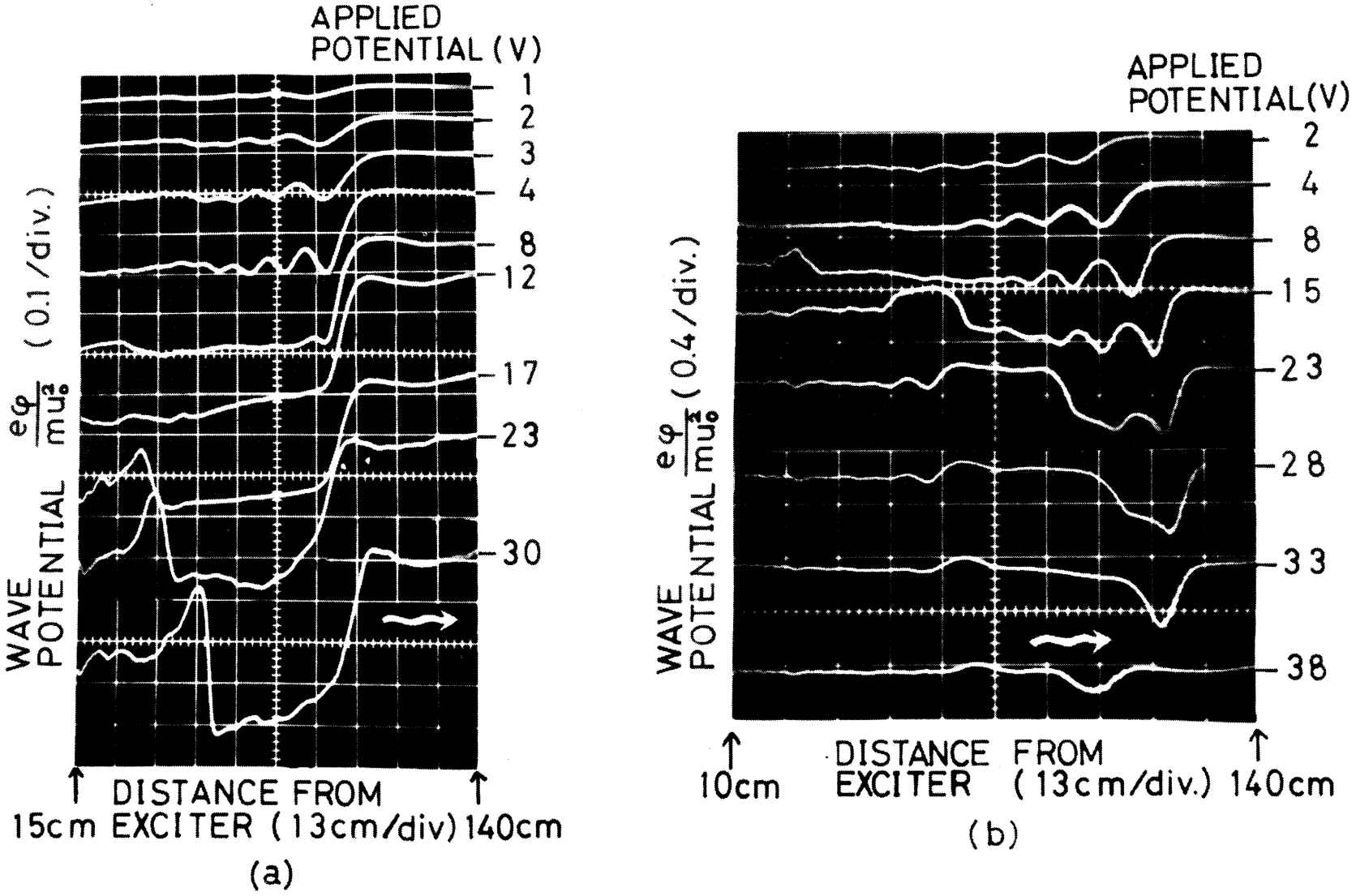
APPLIED
POTENTIAL (V)
1
2
3
4
8
12
17
23
30
WAVE
POTENTIAL $\frac{e\varphi}{mu_0^2}$ (0.1/div.)
15cm
DISTANCE FROM
EXCITER (13cm/div)
140cm
(a)
APPLIED
POTENTIAL(V)
2
4
8
15
23
28
33
38
WAVE
POTENTIAL $\frac{e\varphi}{mu_0^2}$ (0.4/div.)
10cm
DISTANCE FROM
EXCITER (13cm/div.)
140cm
(b)

Fig. 5

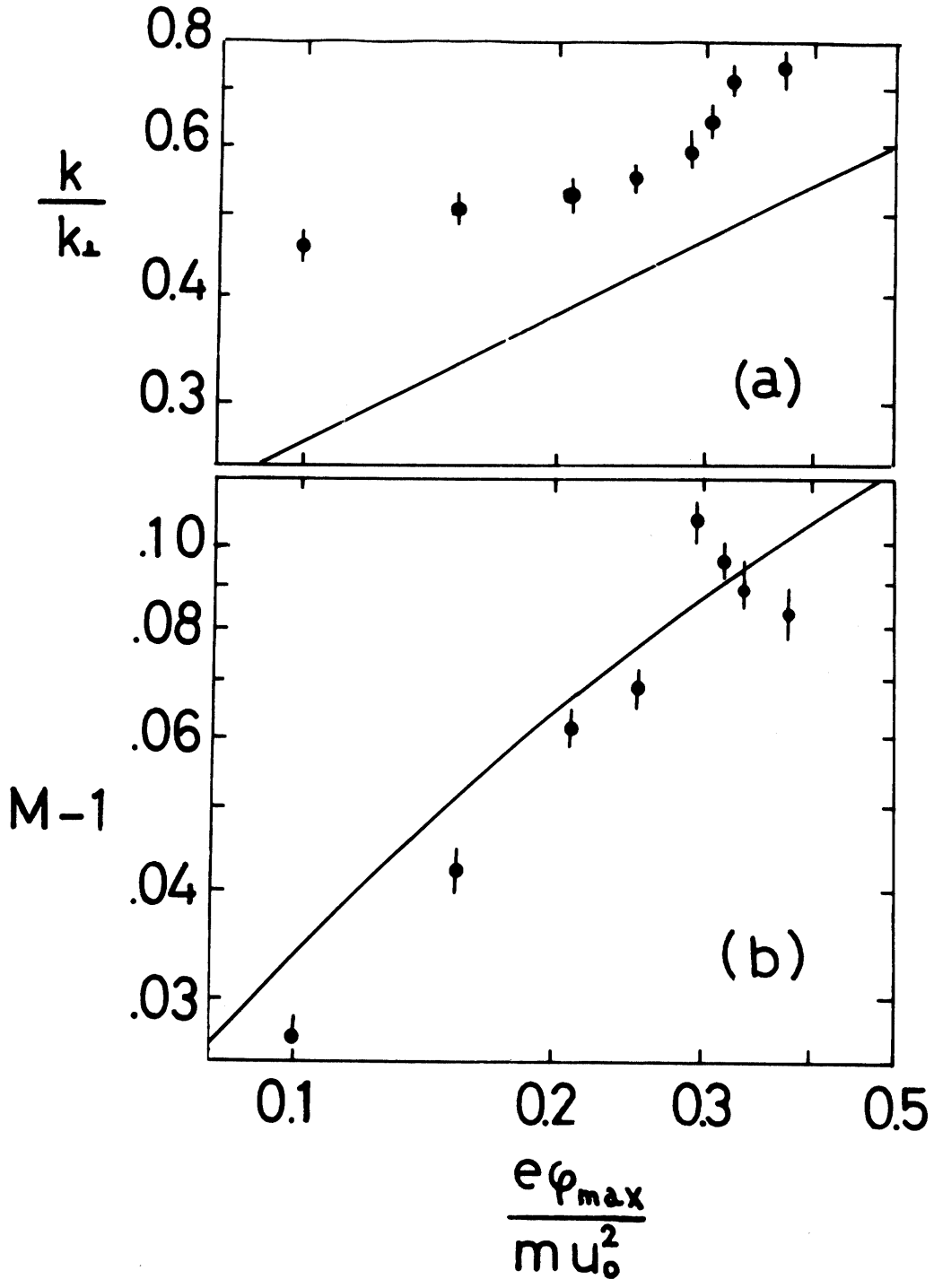

Fig. 6

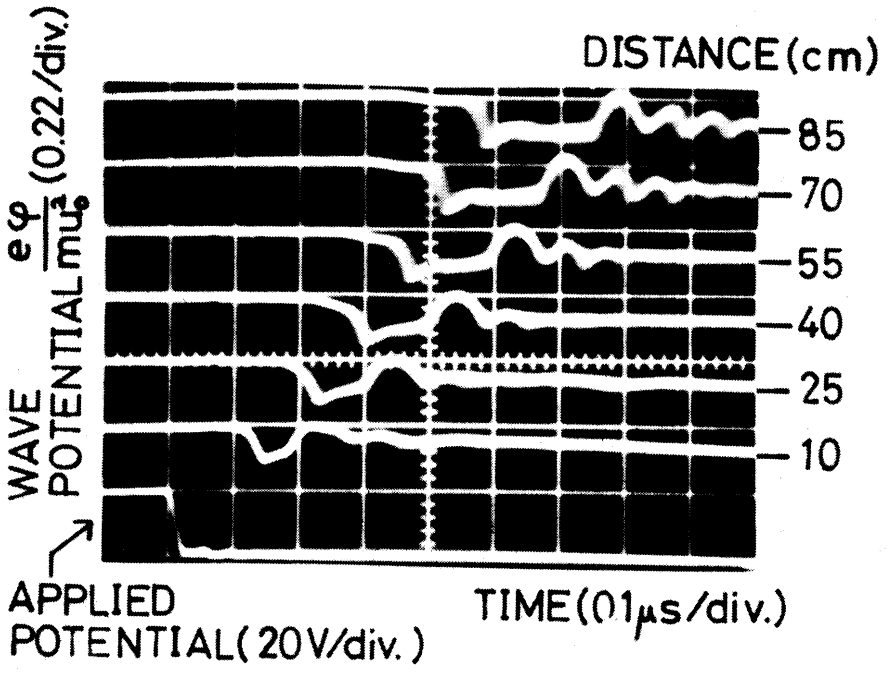
DISTANCE(cm)
85
70
55
40
25
10
WAVE POTENTIAL $\frac{e\varphi}{mu_0^2}$ (0.22/div.)
APPLIED POTENTIAL(20V/div.)
TIME(01μs/div.)

Fig. 7

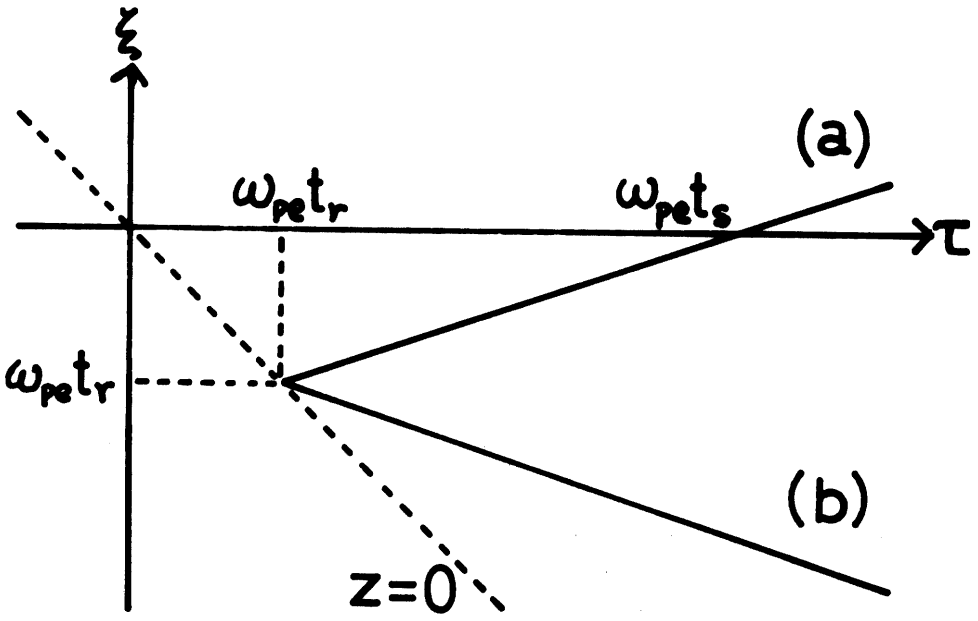

Fig. 8